AD-A042 093 SYRACUSE UNIV N Y DEPT OF ELECTRICAL ENGINEERING F/G 20/3
COUPLING THROUGH ROTATIONALLY SYMMETRIC APERTURES IN CAVITIES O--ETC(U)
JUN 77 H K SCHUMAN, D E WARREN F30602-75-C-0121

UNCLASSIFIED RADC-TR-77-214 NL

| OF |
ADA042093

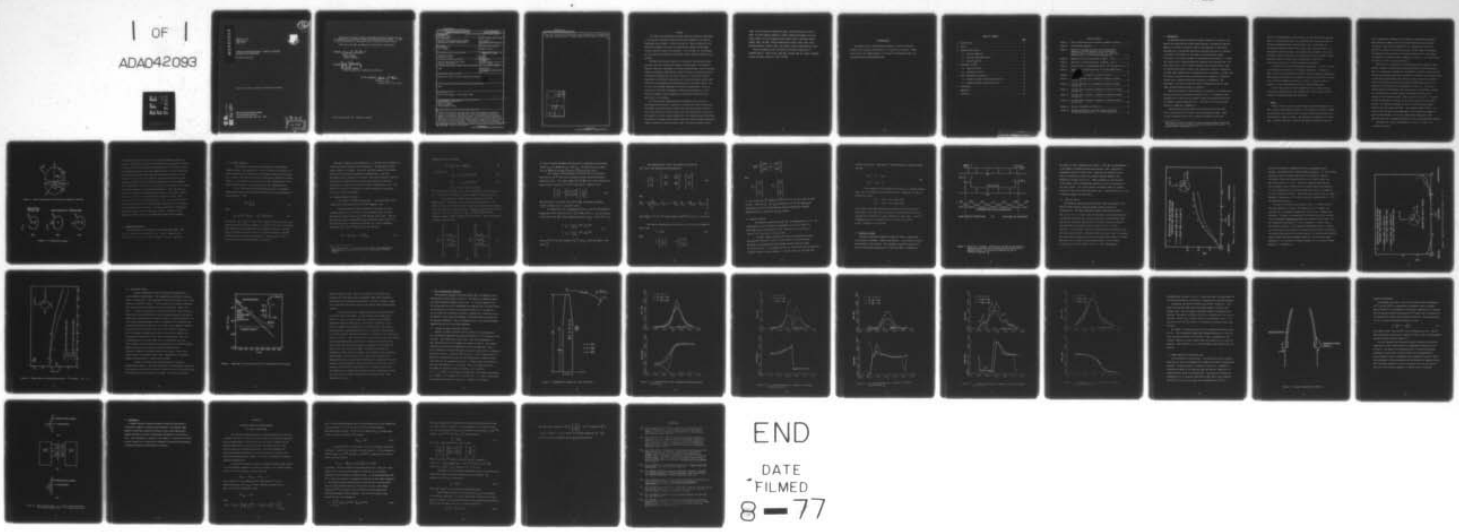

END

DATE FILMED
8-77

(12)
NW

RADC-TR-77-214
Phase Report
June 1977

COUPLING THROUGH ROTATIONALLY SYMMETRIC APERTURES IN CAVITIES OF REVOLUTION

Syracuse University

ROME AIR DEVELOPMENT CENTER
Air Force Systems Command
Griffiss Air Force Base, New York 13441

This report has been reviewed by the RADC Information Office (OI) and is releasable to the National Technical Information Service (NTIS). At NTIS it will be releasable to the general public including foreign nations.

This report has been reviewed and is approved for publication.

APPROVED: Jacob Scherer

JACOB SCHERER
Project Engineer

APPROVED: Joseph J. Naresky

JOSEPH J. NARESKY
Chief, Reliability & Compatibility Division

FOR THE COMMANDER: John P. Huss

JOHN P. HUSS
Acting Chief, Plans Office

Do not return this copy. Retain or destroy.

UNCLASSIFIED
SECURITY CLASSIFICATION OF THIS PAGE (When Data Entered)

REPORT DOCUMENTATION PAGE

READ INSTRUCTIONS BEFORE COMPLETING FORM

1. REPORT NUMBER: RADC-TR-77-214	2. GOVT ACCESSION NO.
3. RECIPIENT'S CATALOG NUMBER	
4. TITLE (and Subtitle): COUPLING THROUGH ROTATIONALLY SYMMETRIC APERTURES IN CAVITIES OF REVOLUTION	5. TYPE OF REPORT & PERIOD COVERED: Phase Report
	6. PERFORMING ORG. REPORT NUMBER: N/A
7. AUTHOR(s): H. K. Schuman, D. E. Warren	8. CONTRACT OR GRANT NUMBER(s): F30602-75-C-0121
9. PERFORMING ORGANIZATION NAME AND ADDRESS: Syracuse University, Syracuse NY 13210	10. PROGRAM ELEMENT, PROJECT, TASK AREA & WORK UNIT NUMBERS: 95670016
11. CONTROLLING OFFICE NAME AND ADDRESS: Rome Air Development Center (RBC), Griffiss AFB NY 13441	12. REPORT DATE: June 1977
	13. NUMBER OF PAGES: 38
14. MONITORING AGENCY NAME & ADDRESS (if different from Controlling Office): Same	15. SECURITY CLASS. (of this report): UNCLASSIFIED
	15a. DECLASSIFICATION/DOWNGRADING SCHEDULE: N/A

16. DISTRIBUTION STATEMENT (of this Report)

Approved for public release; distribution unlimited.

17. DISTRIBUTION STATEMENT (of the abstract entered in Block 20, if different from Report)

Same

18. SUPPLEMENTARY NOTES

RADC Project Engineer: Jacob Scherer (RBC)

19. KEY WORDS (Continue on reverse side if necessary and identify by block number)

Electromagnetic Compatibility
Method of Moments
Aperture Coupling
Electromagnetic Fields

20. ABSTRACT (Continue on reverse side if necessary and identify by block number)

A method for predicting the field penetrating a circumferential opening in a cavity of revolution is described here. This method employs the method of moments and an aperture equivalence theorem. The former permits rotationally symmetric cavities with otherwise arbitrary contours. The latter improves the sensitivity of field computation when the aperture height is tiny and/or points deep within the cavity are sought. This method is evaluated with comparison to classical theory and experiment via application to spherical and cylindrical →

DD FORM 1 JAN 73 1473 EDITION OF 1 NOV 65 IS OBSOLETE

UNCLASSIFIED
SECURITY CLASSIFICATION OF THIS PAGE (When Data Entered)

cavities. Results for a missile-like cavity irradiated by an obliquely incident plane wave are given. A computer program and user manual is available.

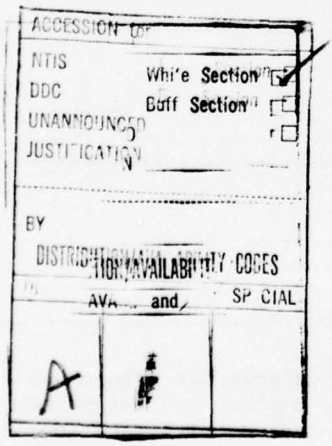

PREFACE

This effort was conducted by Syracuse University under the sponsorship of the Rome Air Development Center Post-Doctoral Program for two Rome Air Development Center tasks. In the first task, Mr. Daniel E. Warren of the Rome Air Development Center was the task project engineer and provided overall technical direction and guidance. In the second, Mr. Jack Edwards was the task project engineer and provided overall technical direction and guidance.

The RADC Post-Doctoral Program is a cooperative venture between RADC and some sixty-five universities eligible to participate in the program. Syracuse University (Department of Electrical Engineering), Purdue University (School of Electrical Engineering), Georgia Institute of Technology (School of Electrical Engineering), and State University of New York at Buffalo (Department of Electrical Engineering) act as prime contractor schools with other schools participating via sub-contracts with the prime schools. The U.S. Air Force Academy (Department of Electrical Engineering), Air Force Institute of Technology (Department of Electrical Engineering), and the Naval Post Graduate School (Department of Electrical Engineering) also participate in the program.

The Post-Doctoral Program provides an opportunity for faculty at participating universities to spend up to one year full time on exploratory development and problem-solving efforts with the post-doctorals splitting their time between the customer location and their educational institutions. The program is totally customer-funded with current projects being undertaken for Rome Air Development Center (RADC), Space and Missile Systems Organization (SAMSO), Aeronautical System Division (ASD), Electronics Systems Division

(ESD), Air Force Avionics Laboratory (AFAL), Foreign Technology Division (FTD), Air Force Weapons Laboratory (AFWL), Armament Development and Test Center (ADTC), Air Force Communications Service (AFCS), Aerospace Defense Command (ADC), HQ USAF, Defense Communications Agency (DCA), Navy, Army, Aerospace Medical Division (AMD), and Federal Aviation Administration (FAA).

Further information about the RADC Post-Doctoral Program can be obtained from Mr. Jacob Scherer, RADC/RBC, Griffiss AFB, NY, 13441, telephone Autovon 587-2543, Commercial (315) 330-2543.

ACKNOWLEDGMENT

The authors wish to thank Professor Bradley J. Strait of Syracuse University for valuable contributions to all aspects of this work. Thanks is due also to Mr. Thomas Baustert of the Rome Air Development Center for assistance during the experiment phase.

TABLE OF CONTENTS

LIST OF FIGURES

1. Introduction

An equivalent aperture excitation method (referred to as BOR3 in this report) for predicting the fields coupled through a rotationally symmetric aperture in a body of revolution (BOR) is described here.* BOR3 has an advantage over a conventional near-field scattering BOR code [2] (referred to as BOR2 in this report) in that BOR3 is characterized by greater sensitivity; tiny field strengths are determined more accurately. In BOR2, the cavity field is found by adding the impressed and scattered field. For small field levels, such as those associated with tiny apertures or those at locations deep within a cavity, this computation involves a subtraction of almost equal numbers with a corresponding loss in accuracy. In BOR3, this difficulty is avoided because the cavity field is computed as a radiation problem once an equivalent aperture excitation is determined. The improvement in accuracy of BOR3 over BOR2 is demonstrated with the open-ended cylinder problem discussed in Section 4.

Based on the method of moments BOR3 is an extension of the widely used BOR work originating at Syracuse University [1,3] . (A computer program implementation of BOR3 [9] also employs a near-field subroutine developed at Lawrence Livermore Laboratory [2].) The details of the Syracuse BOR method are summarized in Appendix A.

There are two principal reasons for restricting a study to BORs. First, many structures of interest can be approximated by BORs. These include streamlined bodies such as aircraft fuselages and missiles.

---

* This method can also be applied to non-rotationally-symmetric-aperture BOR problems although the details become considerably more complex. The general method is described in [5].

Second, the electromagnetic characteristics of a BOR conveniently decouple. That is, a single Fourier mode, or circumferentially varying sinusoid, of excitation (impressed field, aperture field, etc.) excites only the corresponding mode of response (far or near field, current density, etc.). This permits significant savings in computer time and memory. With modal decoupling a matrix formulation of the problem results in a number of small matrices to deal with rather than one huge matrix. The latter often arises with use of an arbitrary surface formulation.

In Section 2, the theory behind BOR3 is described. In Section 3, BOR3 is detailed as an extension of the Syracuse BOR method. In Section 4, BOR3 is evaluated by comparison with BOR2, classical methods and experiment. These methods are applied to both spherical and finite-cylindrical cavities with rotationally symmetric apertures. Finally, in Section 5 BOR3 is applied to a thin circumferential slot in a missile-shaped body.

A user's description of a BOR3 computer code and a Fortran source listing with example printout are available [9]. This version of BOR3 is limited to $\hat{\theta}$-polarized plane-wave excitation.

2. Theory

Figure 1 shows a plane wave incident upon a perfectly conducting BOR with a rotationally symmetric aperture. The surface of a BOR may be formed by constructing any contour in the y-z plane, called the generating curve, and rotating it about the z-axis. The cylinder and conesphere are typical BORs. The basic treatment of BORs by the method of moments has been set

forth by Harrington and Mautz [3] for radiation and scattering problems. They developed a computer code for this method which has proven useful in solving a large class of problems [1,3]. Essentially, the task is reduced to inverting a set of matrices each of order equal to the number of expansion functions applied to the BOR generating curve. Each matrix corresponds to a different Fourier component, or mode, n, of circumferential variation of fields and current densities.

The basis for the adaptation of the Harrington-Mautz (Syracuse) BOR method to aperture coupling via the equivalent aperture excitation method, BOR3, is an equivalence theorem due to Schelkunoff [4] which states that the original problem containing sources external to the body, can be replaced with an equivalent problem having only aperture current sources for excitation. Figure 2 illustrates this where the original problem depicted in (a) is equivalent to the sum of the two problems in (b) and (c). In (b), the induced surface current density $\underset{\sim}{J}^{\circ}$ in the vicinity of the aperture is found for the apertureless (replace aperture with conductor) body in the presence of the external sources. Then, as shown in (c), $\underset{\sim}{J}^{A} = -\underset{\sim}{J}^{\circ}$ becomes an aperture excitation resulting in the internal fields of the original problem. For BORs both problems (b) and (c) can be solved by proper modification of the Syracuse Method. This modified method is BOR3. It is shown in [5] that BOR3 is also applicable to non-rotationally-symmetric-aperture BOR problems, with all the computational advantages of BOR modeling maintained, although the details are then considerably more complex.

The method for solving the problems of (b) and (c) (Figure 2) is outlined as follows:

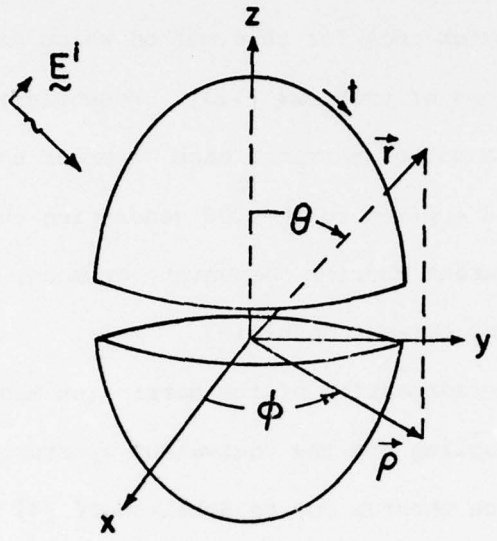

Figure 1. Body of Revolution with Rotationally Symmetric Aperture.

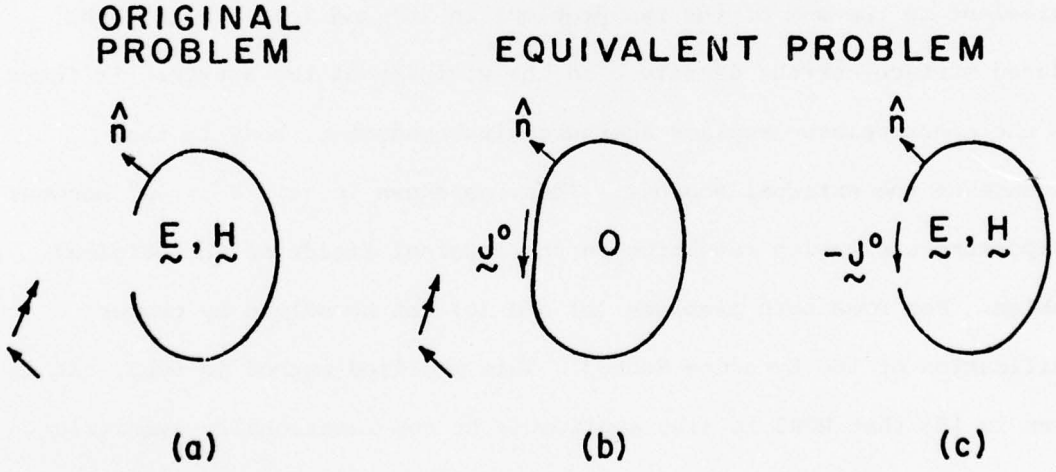

Figure 2. An Equivalence Theorem

The problem depicted by Figure 2b is a straight-forward BOR scattering problem. The problem of Figure 2c is solved by first replacing the current excitation $\underset{\sim}{J}^A$ with an equivalent $\underset{\sim}{E}$-field excitation. The latter is found by dividing the aperture into thin ribbon-like cells, or ports, along the generating curve, short-circuiting them, and exciting each one in turn with a bi-directed (since the surface is two-dimensional) $\underset{\sim}{E}$-field, each component of which is unity across the excited port and zero elsewhere. The circumferential variation of each port-$\underset{\sim}{E}$-field excitation is, of course, the Fourier component or mode under consideration. Thus, for each port $\underset{\sim}{E}$-field, the bi-directed current density induced at every port is easily obtained by solving a straight-forward BOR radiation problem. This results in an "aperture admittance matrix", $[y^A]$. The inversion of $[y^A]$ and post-multiplication by the column matrix representation of $\underset{\sim}{J}^A$ results in the desired $\underset{\sim}{E}$-field excitation. The latter approximates the aperture tangential $\underset{\sim}{E}$-field, $\underset{\sim}{E}^A$, of the original problem. Excitation of the aperture with $\underset{\sim}{E}^A$ is, again, a straight-forward BOR radiation problem.

3. Computational Details

The BOR3 method is an extension of the Syracuse BOR method. The latter is detailed in references [1,2,3]. A brief summary of the formulations and notation in these references is given in Appendix A.

3.1 Aperture Modelling

The aperture is considered as divided into P rotationally symmetric ports. For simplicity the choice of location and extent of a port is constrained to contain only one triangle expansion function peak. The triangle functions referred to are those which, divided by the BOR radius, ρ, are chosen to give a piece-wise linear approximation to the current density along the generating curve of the apertureless BOR.

The n^{th} mode aperture $\underset{\sim}{E}$-field excitation, $\underset{\sim}{E}^A$, is determined numerically by subsection expansion where each subsection corresponds to an aperture port. Thus

$$\underset{\sim}{E}^A = \sum_{p=1}^{P} \underset{\sim}{E}_p \tag{1}$$

where

$$\underset{\sim}{E}_p = E_p^t \, e^{jn\phi} \, X_p^t(t)\hat{t} + E_p^\phi \, e^{jn\phi} \, X_p^\phi(t) \, \hat{\phi} \tag{2}$$

Here E_p^t and E_p^ϕ are the n^{th} mode t and ϕ expansion function coefficients respectively of the p^{th} port $\underset{\sim}{E}$-field, and $X_p^t(t)$, $X_p^\phi(t)$ are the functions which describe the t dependence of these expansion functions. Once E_p^t and E_p^ϕ are known, the cavity field can be found by solving an aperture radiation problem as outlined in Appendix A. The remainder of this section deals with the determination of E_p^t and E_p^ϕ

Note that a subscript (or superscript) n is omitted from the symbols of various quantities arising in this development. The dependence on mode number, however, is assumed. Due to the rotational symmetry the derived quantities for each mode are determined independently. Thus this development can be repeated for each mode. The total response is then the sum of all the individual modal (positive and negative n) responses each having a ϕ dependence given by the complex exponentials in (2). The addition of a positive and negative n response exhibits the equivalent $\sin(n\phi)$ or $\cos(n\phi)$ dependence.

3.2 Aperture Admittance Matrix

The elements of $[y^A]$ are derived here. The matrix $[y^A]$ relates column vector representations of $\underset{\sim}{E}^A$ and $\underset{\sim}{J}^A$ [equation (12)].

The pq^{th} element of $[y^A]$ is determined by exciting the short-circuited aperture at the p^{th} port with an arbitrary value of $\underset{\sim}{E}_p$ and recording the current density $\underset{\sim}{J}_q$ flowing through the q^{th} port. With the BOR excited by $\underset{\sim}{E}_p$ the generalized voltage excitation column vector* can be partitioned into a t-component sub-vector, $\vec{V}_p^{\,t}$, and a ϕ-component sub-vector, $\vec{V}_p^{\,\phi}$. The j^{th} element of $\vec{V}_p^{\,t}$ has the form

$$V_j^t = \langle W_{nj}^t , E_p \rangle = 2\pi E_p^t F_{j,p}^t \qquad (3)$$

---

* Appendix A reviews the formulations (and defines the symbolism) for determining a BOR current density given an impressed or aperture $\underset{\sim}{E}$-field.

Similarly for the ϕ-component,

$$V_j^{\phi} = \langle W_{nj}^{\phi} , E_p \rangle = 2\pi E_p^{\phi} F_{j,p}^{\phi} \tag{4}$$

In (3) and (4),

$$F_{j,p}^{t} = \int_{gc} \rho f_j(t)\, X_p^{t}(t)dt \tag{5}$$

$$F_{j,p}^{\phi} = \int_{gc} \rho f_j(t)\, X_p^{\phi}(t)dt \tag{6}$$

$\rho f_j(t)$ = the j^{th} triangle function

the weighting functions W_{nj}^{t} , W_{nj}^{ϕ} , and the symmetric product denoted by "< >" are defined in Appendix A, and gc stands for "generating curve".

Let j_p denote the triangle function with peak at the p^{th} aperture port. Then because of the aforementioned constraints on the extent of a port the functions $X_p^{t}(t)$ and $X_p^{\psi}(t)$ are zero beyond the peaks of the j_p-1 and j_p+1 triangle functions. Therefore, $F_{j,p}^{t}$ and $F_{j,p}^{\phi}$ are non-zero only for $j = j_p - 1$, $j = j_p$, and $j = j_{p+1}$. (Further considerations concerning choice of $X_p^{t}(t)$ and $X_p^{\phi}(t)$ are given later.) Thus the excitation sub-vectors have the form

$$\vec{V}_p^{\,t} = \begin{bmatrix} 0 \\ \cdot \\ \cdot \\ \cdot \\ 0 \\ 2\pi E_p^{t} F^{t}_{j_p-1,p} \\ 2\pi E_p^{t} F^{t}_{j_p,p} \\ 2\pi E_p^{t} F^{t}_{j_p+1,p} \\ 0 \\ \cdot \\ \cdot \\ \cdot \\ 0 \end{bmatrix} \qquad \vec{V}_p^{\,\phi} = \begin{bmatrix} 0 \\ \cdot \\ \cdot \\ \cdot \\ 0 \\ 2\pi E_p^{\phi} F^{\phi}_{j_p-1,p} \\ 2\pi E_p^{\phi} F^{\phi}_{j_p,p} \\ 2\pi E_p^{\phi} F^{\phi}_{j_p+1,p} \\ 0 \\ \cdot \\ \cdot \\ \cdot \\ 0 \end{bmatrix} \tag{7}$$

Of course for ports located at the junctions of generating curve and axis (poles) F_{j_p-1} is absent for $j_p = 1$ and F_{j_p+1} is absent for $j_p = nm$ where nm= the number of triangle functions on the generating curve.

The "current" flowing through the q^{th} port due to a localized excitation at the p^{th} port can be obtained from the generalized network admittance matrix. The latter relates $\vec{V}_p^{\,t}$ and $\vec{V}_p^{\,\phi}$ to the t and ϕ generalized network current subvectors $\vec{I}^{t}$ and $\vec{I}^{\phi}$ respectively, (Appendix A) by

$$\begin{bmatrix} \vec{I}^{t} \\ \vec{I}^{\phi} \end{bmatrix} = -\left[\begin{array}{c|c} [Y^{tt}] & [Y^{t\phi}] \\ \hline [Y^{\phi t}] & [Y^{\phi\phi}] \end{array}\right] \begin{bmatrix} \vec{V}_p^{\,t} \\ \vec{V}_p^{\,\phi} \end{bmatrix} \tag{8}$$

The minus sign in (8) arises since $\vec{V}_p^{\,t}$ and $\vec{V}_p^{\,\phi}$ correspond to aperture (total) $\underset{\sim}{E}$-fields and not "impressed" fields.

For simplicity, the correspondence between $\underset{\sim}{J}_q$ and the corresponding generalized current sub-vectors $\vec{I}_q^{\,t}$, $\vec{I}_q^{\,\phi}$ is made only at $t = t_q$, the location of the peak of the j_q^{th} triangle expansion function $\rho f_{j_q}(t)$. Thus, at $t = t_q$,

$$\begin{aligned} \hat{t} \cdot \underset{\sim}{J}_q &= \left(\frac{1}{\rho_q} I_{j_q}^{t} \right) e^{jn\phi} = J_q^{t} e^{jn\phi} \\ \hat{\phi} \cdot \underset{\sim}{J}_q &= \left(\frac{1}{\rho_q} I_{j_q}^{\phi} \right) e^{jn\phi} = J_q^{\phi} e^{jn\phi} \end{aligned} \tag{9}$$

where $I_{j_q}^{t(\phi)}$ is the j_q^{th} element of $\vec{I}_q^{\,t(\phi)}$ and ρ_q is the BOR radius to the point t_q.

The combination of (7,8,9) and removal of all but the j_q^{th} rows in the admittance matrix results in

$$\begin{bmatrix} J_q^t \\ J_q^\phi \end{bmatrix} = \begin{bmatrix} y_{q,p}^{tt} & y_{q,p}^{t\phi} \\ y_{q,p}^{\phi t} & y_{q,p}^{\phi\phi} \end{bmatrix} \begin{bmatrix} E_p^t \\ E_p^\phi \end{bmatrix} \tag{10}$$

Here

$$y_{q,p}^{ab} = \frac{-2\pi}{\rho_q} \left[Y_{j_q, j_p - 1}^{ab} F_{j_p - 1, p}^{b} + Y_{j_q, j_p}^{ab} F_{j_p, p}^{b} + Y_{j_q, j_p + 1}^{ab} F_{j_p + 1, p}^{b} \right] \tag{11}$$

where $Y_{\alpha,\beta}^{ab}$ = the α^{th} row, β^{th} column element of $[y^{ab}]$ and ab=tt, tϕ, ϕt, and $\phi\phi$.

The aperture admittance relationship for all P ports then becomes,in matrix form,

$$\vec{j} = [y^A]\vec{e} \tag{12}$$

where

$$\vec{j} = \begin{bmatrix} \vec{j}^t \\ - - \\ \vec{j}^\phi \end{bmatrix} \qquad \vec{e} = \begin{bmatrix} \vec{e}^t \\ - - \\ \vec{e}^\phi \end{bmatrix}$$

$$[y^A] = \left[\begin{array}{c|c} [y^{tt}] & [y^{t\phi}] \\ \hline [y^{\phi t}] & [y^{\phi\phi}] \end{array}\right]$$

Here

$$\vec{j}^a = \begin{bmatrix} J_1^a \\ \cdot \\ \cdot \\ \cdot \\ J_P^a \end{bmatrix} \qquad \vec{e}^a = \begin{bmatrix} E_1^a \\ \cdot \\ \cdot \\ \cdot \\ E_P^a \end{bmatrix}$$

$a = t$ or ϕ and the q,p^{th} element of $[y^{ab}]$, $ab = tt$, $t\phi$, ϕt, or $\phi\phi$, is given by (11). Note that J_q^t and J_q^ϕ are defined as in (9) but with $\underset{\sim}{J}_q$ now representing the total current density flowing through port q (entire aperture excited as opposed to only $\underset{\sim}{E}_p$ present).

3.3 Aperture E-Field

The aperture tangential $\underset{\sim}{E}$-field, $\underset{\sim}{E}^A$, is represented by (1, 2). The coefficients in (2) are given by the solution to (12) for $\vec{e}$ when $\vec{j}$ is the column vector representation of $\underset{\sim}{J}^A$. The latter is known from the solution to the apertureless body problem.

The $X_p^t(t)$, $X_p^\phi(t)$ functions are chosen to be essentially pulses with special consideration given to their form at the aperture edges. One pulse is associated with each triangle function that has a peak within the aperture. These aperture pulses are specified by the corresponding triangle expansion function numbers, i, and the lower Δt_i^-, and upper Δt_i^+,

extents of the pulse. Note Figure 3. The constraints on the pulse width are that

$$\Delta t_i^- < t_i - t_{i-1}$$
$$\Delta t_i^+ < t_{i+1} - t_i \qquad (13)$$

The $\hat{\phi}$-component of $\underset{\sim}{E}^A$ should be zero along a ϕ = constant aperture edge, and the $\hat{t}$-component becomes infinite there. Therefore, the X_p^ϕ are modified by setting

$$\Delta t^- \rightarrow \Delta t^-/2 \quad \text{at a lower edge}$$
$$\Delta t^+ \rightarrow \Delta t^+/2 \quad \text{at an upper edge}$$

and the X_p^t are modified by doubling the amplitude of the portion of a pulse closest to an edge (the Δt^- portion of a pulse located at a lower edge and the Δt^+ portion of a pulse located at an upper edge). Thus the $\hat{t}$-component functions at aperture edges are really step pulses. Figure 3 examplifies these pulses.

4. Evaluation of BOR3

Cavities of convenient shape were chosen in order to compare BOR3 with classical techniques. Results with spherical and cylindrical cavities are presented in this section. Also included are results obtained from both the conventional application of a BOR code, BOR2, and experiment.

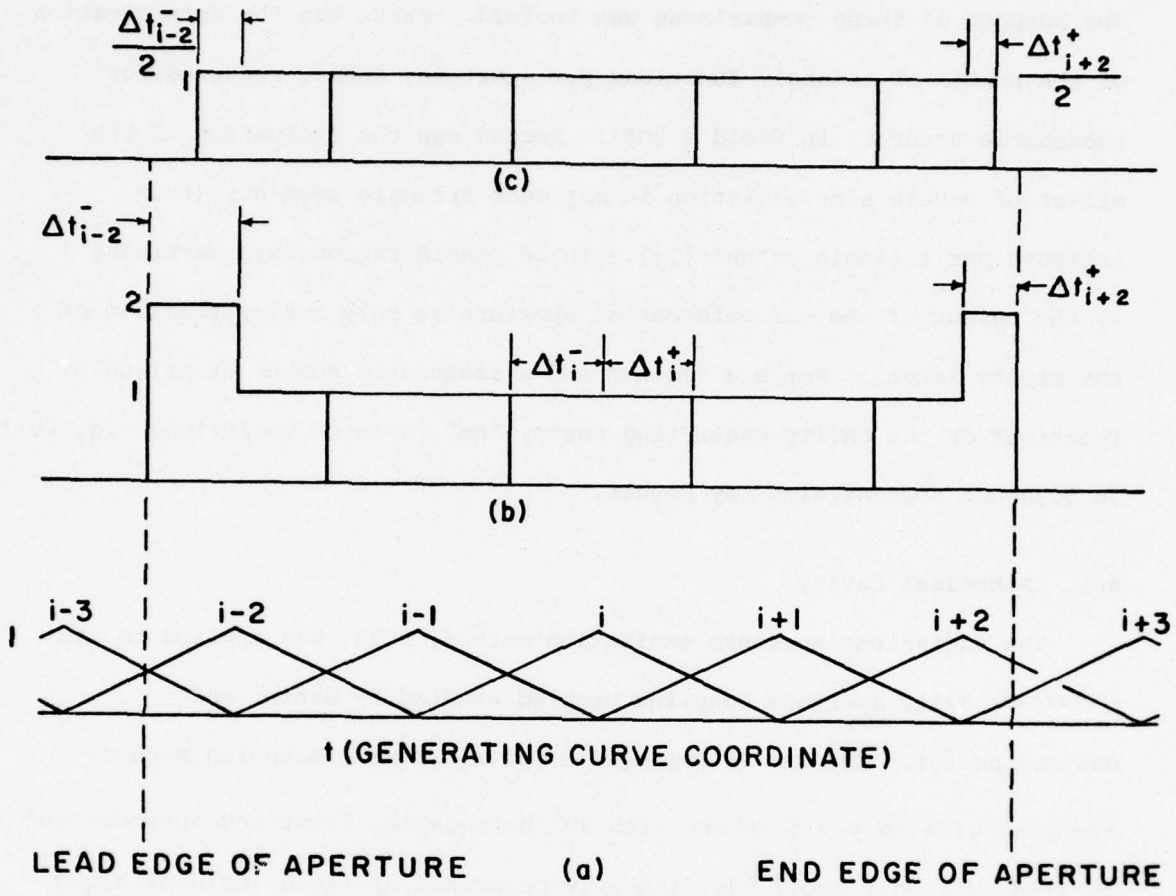

Figure 3. Typical (a) Triangle Functions for Current Density Expansion Along BOR Generating Curve and Modified Pulse Functions for Aperture $\underset{\sim}{E}$-field (b) $\hat{t}$-directed Component X_p^t and (c) $\hat{\phi}$-directed Component X_p^{ϕ}.

The purpose of these comparisons was twofold. First was the determination of the number of triangle functions per aperture, "nam", required for reasonable accuracy in field (~20%). Second was the evaluation of the effect of severe size variation in adjacent triangle segments (four segments per triangle extent [1]). These considerations are pertinent if the height of the circumferential aperture is only a tiny fraction of the cavity length. For a given nam and a reasonable number of triangle functions on the cavity generating curve, "nm", a large variation, e.g. 10:1, in adjacent segment size may result.

4.1. Spherical Cavity

The equivalent aperture excitation method, BOR3, was applied to the spherical cavity aperture coupling problem studied by Senior and Desjardins [6]. The latter employed a spherical mode matching method. The case of a ka = 2.5 sphere with 30° half-angle, front-end aperture and excited by a unit amplitude, linearly polarized, $\underset{\sim}{E}$-field incident along the axis and toward the aperture side of the body is shown in Figure 4. The magnitude of the internal $\underset{\sim}{E}$-field along the axis is plotted. Only the n = ±1 mode (sinϕ, cosϕ) was excited because the impressed plane wave was axially incident. The BOR3 result for a total of nm = 15 triangle functions along the generating curve of the apertureless sphere is in good agreement with the spherical mode matching result. Five of these triangles traversed the aperture (nam = 5). This necessitated a

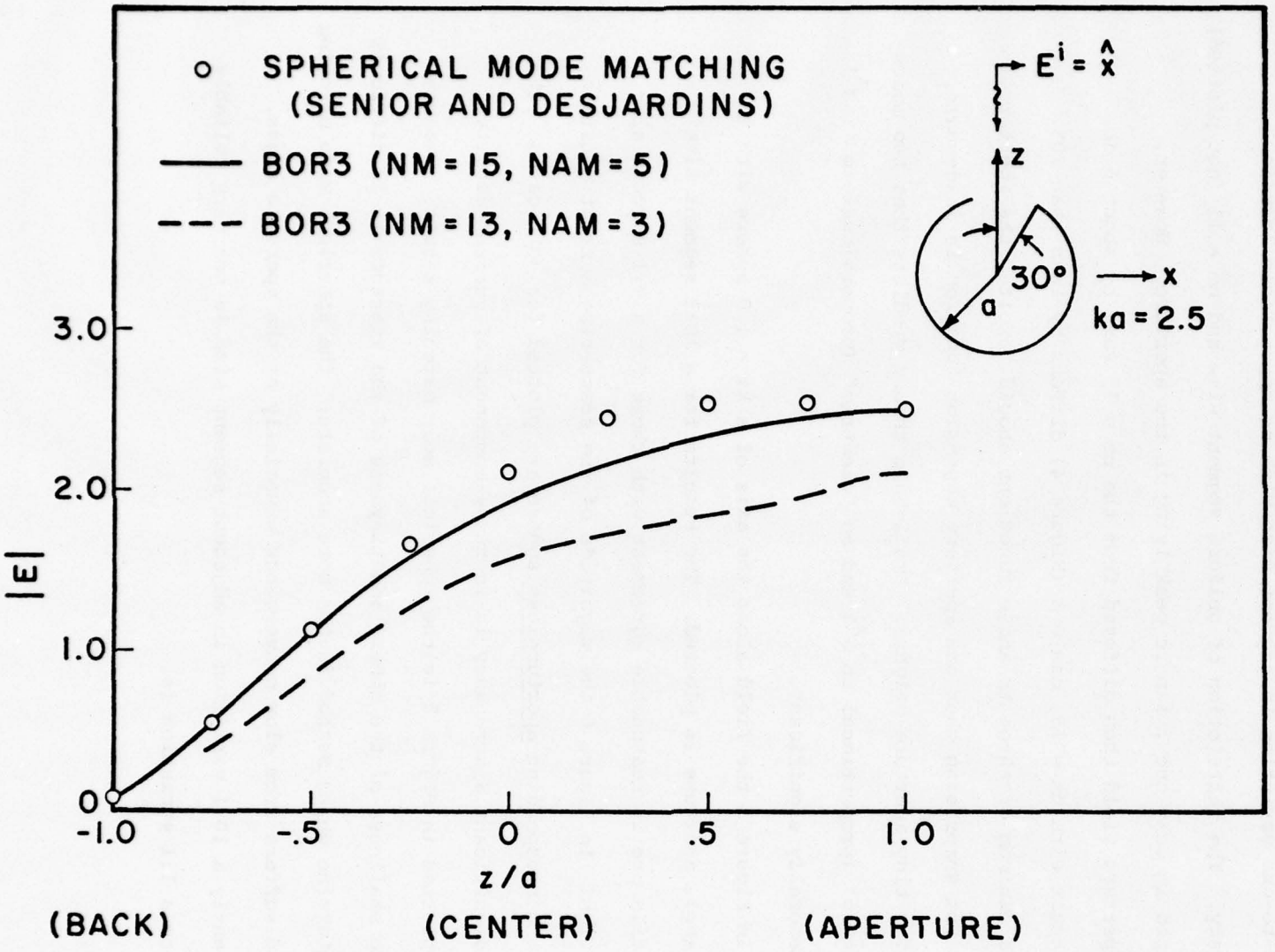

Figure 4. Amplitude of E-Field Along Axis of Sphere. ka = 2.5.

three-to-one variation in segment size with no appreciable loss in accuracy. The restriction of uniform segment size and nm = 11 (not plotted) resulted in only one triangle peak lying in the aperture. However, the aperture field then differed from the nm = 15 case by about 6 db. The result with nm = 13, nam = 3 (Figure 4) differs by less than 20%. Thus a minimum of three triangle functions should "excite" the aperture. It is not surprising that one aperture expansion function is inadequate, even for tiny aperture heights. Small-Hole theory predicts that two modes- a "magnetic" (proportional to $\underset{\sim}{J}^A$) and an "electric" (proportional to $\nabla \cdot \underset{\sim}{J}^A$) - are generally significant.

In Figure 5 the field along the axis of a ka = 1.0 sphere with 10° half angle aperture is plotted. The results for a 10:1 segment size variation are in reasonable agreement with those for a 2:1 segment size variation. In Figure 6 the magnitude of the scattering current densities on the corresponding <u>apertureless</u> sphere are plotted for both cases. The most significant discrepancy is in the $\hat{\phi}$-component of current density. Also plotted in Figure 5 is the spherical mode matching result. Because of the smallness of the sphere and tinyness of the aperture it is difficult to determine which method is the more accurate; the spherical mode matching method suffers from slow convergence especially at the aperture edges. Apparently a 10:1 variation in adjacent segment size is not very reliable whereas a 3:1 variation is.

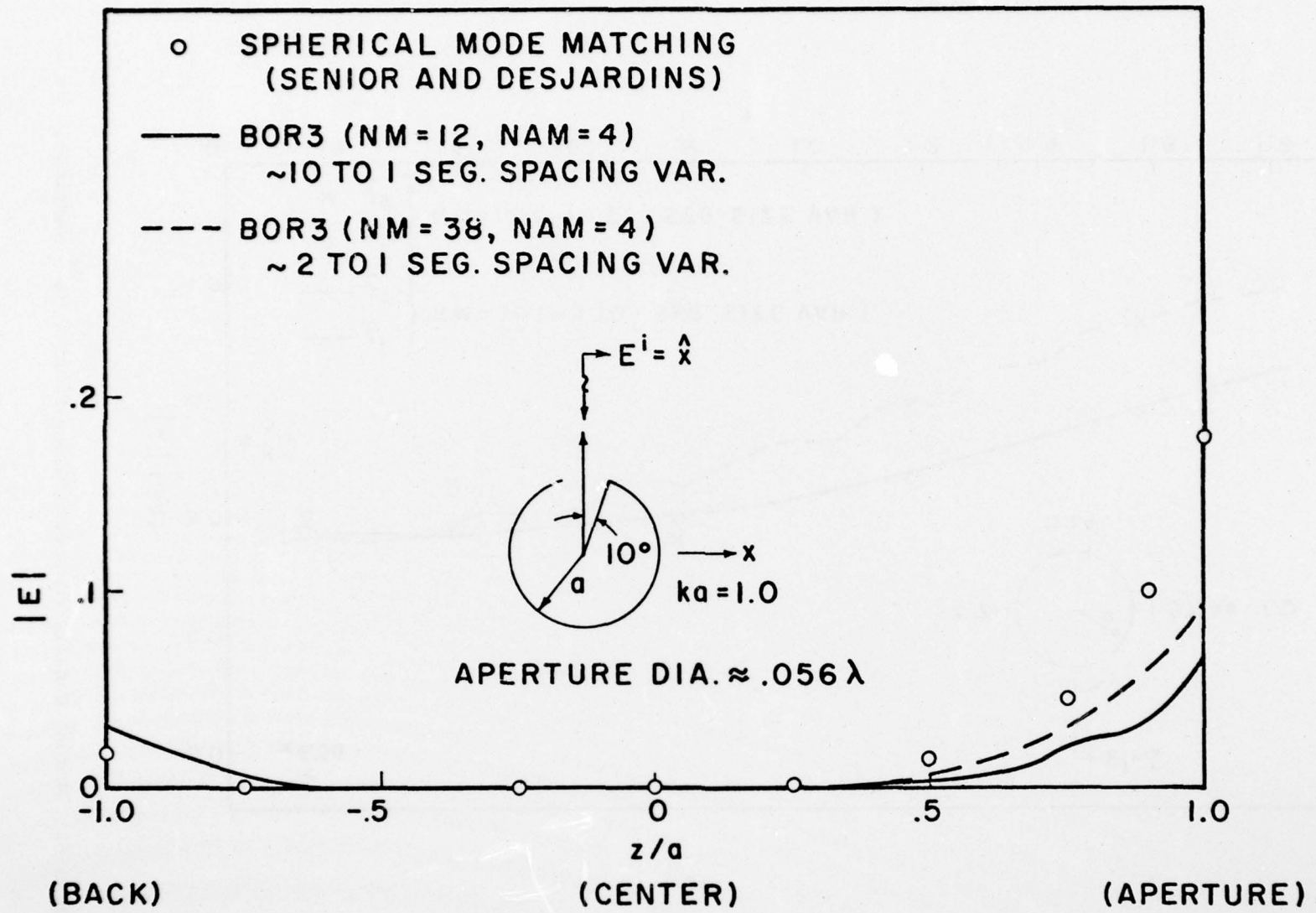

Figure 5. Amplitude of E-Field Along Axis of Sphere. ka = 1.0.

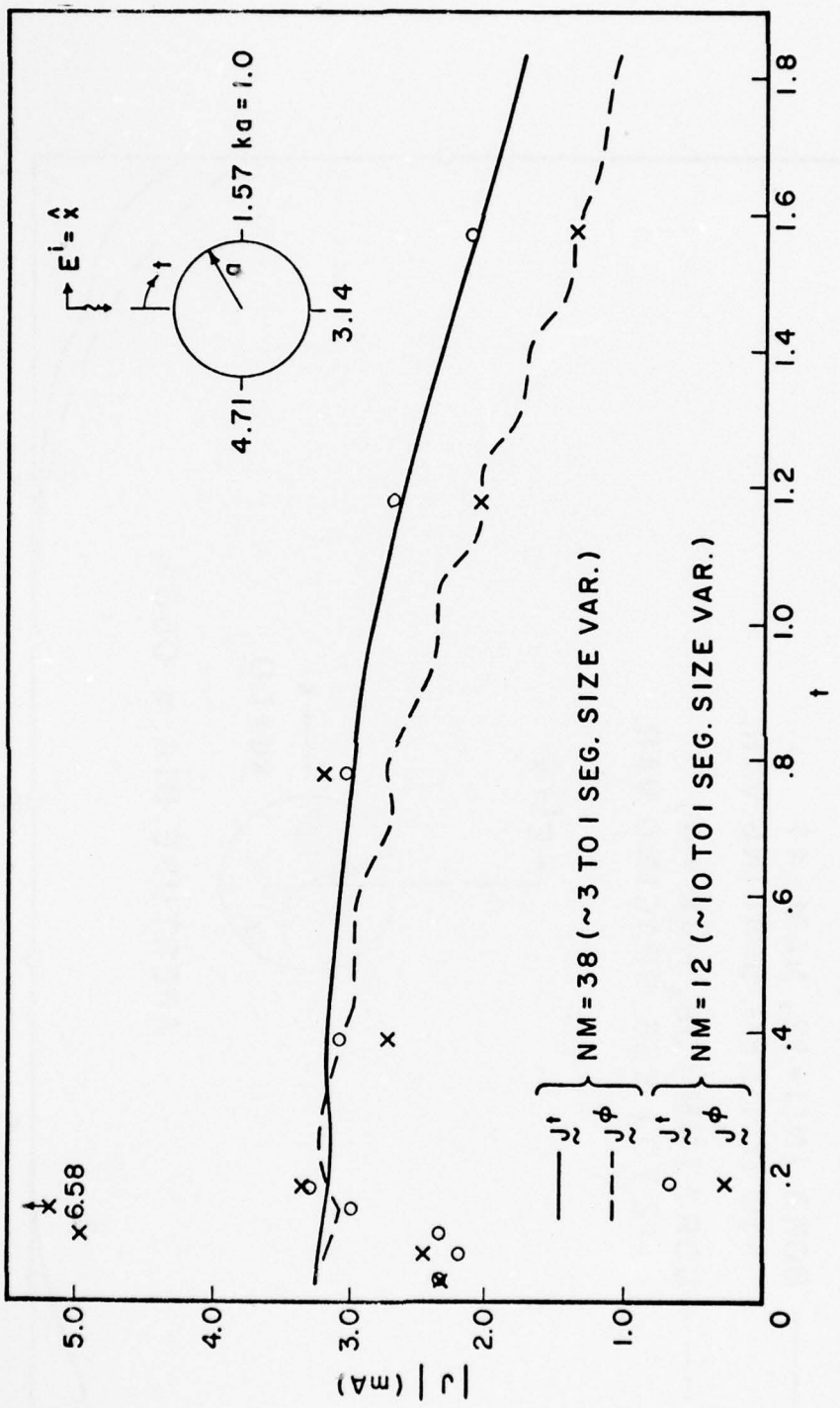

Figure 6. Current Density on Apertureless Sphere ($e^{j\phi}$ Varying). ka = 1.0.

4.2 Cylindrical Cavity

Further evaluation of BOR3 was obtained with application to an open-ended cylinder problem. The comparison was with BOR2, classical theory, and experiment. The magnitude of the $\underset{\sim}{E}$-field along the axis of the cylinder is plotted in Figure 7. The excitation was a linearly polarized unit plane wave axially incident on the open-ended side. Again, only the $n = \pm 1$ mode was excited due to the axial incidence. The conventional application of the BOR code, BOR2, and the equivalent aperture excitation method, BOR3, agree well to a distance of about $.2\lambda$ into the cylinder. The scale factor difference between them is attributed to the different ways in which each models the aperture; an increase in the number of expansion functions should bring both methods into better agreement. Beyond $.2\lambda$ into the cylinder the BOR2 result tends to level off and approach the "closed body" (apertureless) result which is also plotted. This is to be expected since the "closed body" field is essentially the error field (ideally zero) resulting from the approximations in method-of-moment modelling and the errors associated with the aforementioned (Section 1) addition of impressed and scattered fields. BOR3 is not limited by the "closed body" field. Thus it demonstrates a minimum of perhaps 20dB improvement in sensitivity over BOR2.

A check on the BOR3 result was obtained from a classical waveguide-mode analysis. The modal components were determined by requiring zero tangential $\underset{\sim}{E}$-field on the cylinder surface except in the aperture where the $\underset{\sim}{E}$-field predicted by BOR3 was prescribed. Five electric and five

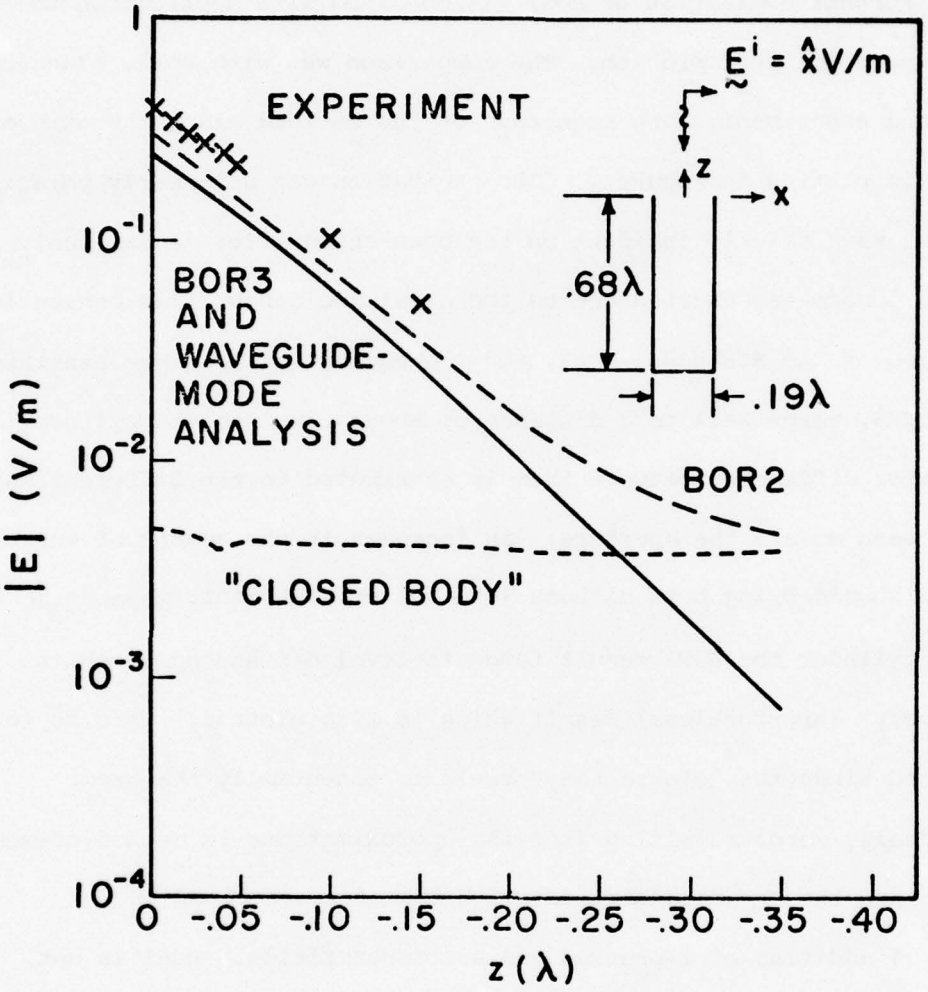

Figure 7. Amplitude of $\underset{\sim}{E}$-Field Along Axis of an Open-Ended Finite Cylinder.

magnetic modes were used. Due to the thinness of the cylinder (the frequency was well below cutoff) the dominant mode alone essentially resulted in the fields beyond the aperture. As shown in Figure 7, there is no observable difference between the cylindrical mode matching method and BOR3.

A further check on the computational methods was obtained with an anechoic chamber experiment. An electrically short diode-loaded probe and a high resistance transmission line were used to minimize measurement apparatus interference. The probe was mounted on a non-metallic "plunger" with placement holes radially spaced. The plunger was mounted on a calibrated dielectric rod. In this way, all positions of the probe could be determined accurately. A sampling of the results are plotted in Figure 7. They are adjusted to account for the dielectric support which, experiment showed, increases the observable field by about 20%. There is good agreement between theory and experiment for distances of about .15λ or less into the cylinder. For greater distances the experimental results were not reliable, and, therefore, they are omitted from the graph. The reason for this is that at the .15λ point the dominant-mode field was approximately 30dB below the impressed field, and harmonics of the fundamental, which were closer to or above the cut-off frequency of the "guide," became significant. Attempts at filtering the transmitter to suppress these harmonics could not appreciably extend the curve due to the severe attenuation of the dominant mode at the fundamental frequency.

5. Thin Circumferential Aperture

The equivalent aperture excitation method, BOR3, was applied to the missile-like structure shown in Figure 8. The aperture is modelled simply as a small separation between two sections. It is noted, however, that actual apertures are often considerably more complex since the section walls can overlap at the junction as indicated in Figure 14, or the aperture can be filled with a dielectric material or sealed with a conductive putty. An extension of the foregoing technique is available which can account for the aperture complexity. This is discussed later in this section although computations have not as yet been performed.

5.1 Oblique Incidence Plane Wave Excitation

Figures 9-13 show the $\underset{\sim}{E}$-field in the vicinity of the aperture for a unit, $\hat{\theta}$-polarized impressed field arriving from the $\theta = 45°$ direction in the x-z plane. Each figure plots three lines. Each line corresponds to a path indicated by one of the dashed lines shown in Figure 8. The azimuth orientation of each path corresponds to that of peak amplitude. The ρ- and z- components of $\underset{\sim}{E}$-field (E_ρ^n, E_z^n) each vary as $\cos n\phi$, and the ϕ-component, E_ϕ^n, varies as $\sin n\phi$. Plots are shown for the n = 0 and 1 modes except for E_ϕ^0 which is identically zero due to the $\hat{\theta}$-polarization of impressed field. Other modes are not presented since the n = 2 modal fields were found to be more than 20db below the n = 0,1 fields. This is not surprising since the number of significant modes is limited to all n such that $|n| \leq 1 + C_\lambda$ where C_λ is the largest circumference of the body in wavelengths [1]. However, it is interesting to note that the n = 1 mode is significant even though the structure is quite thin. Although the sinusoidal

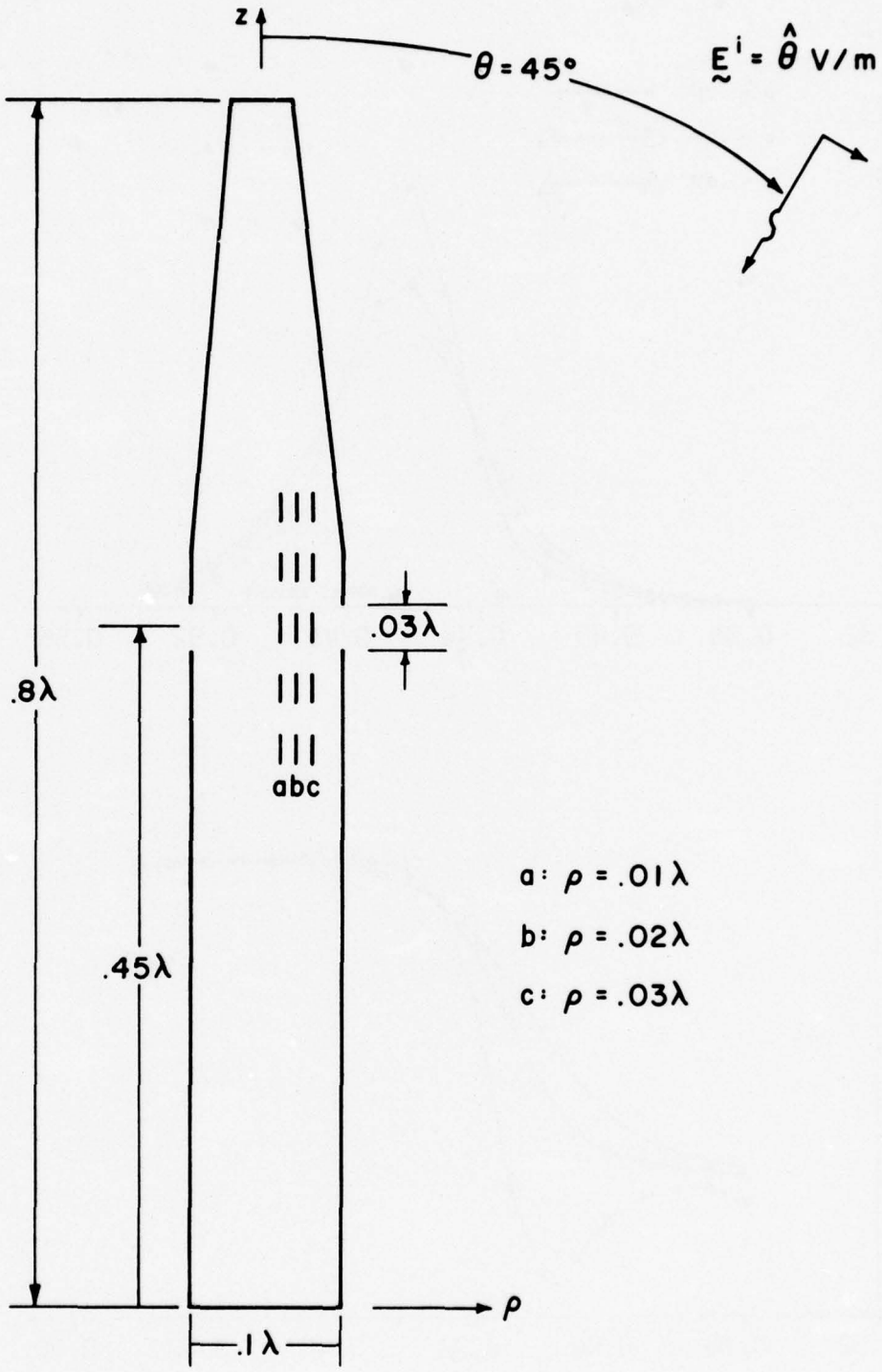

Figure 8. Circumferential Opening in a Long Thin Cavity.

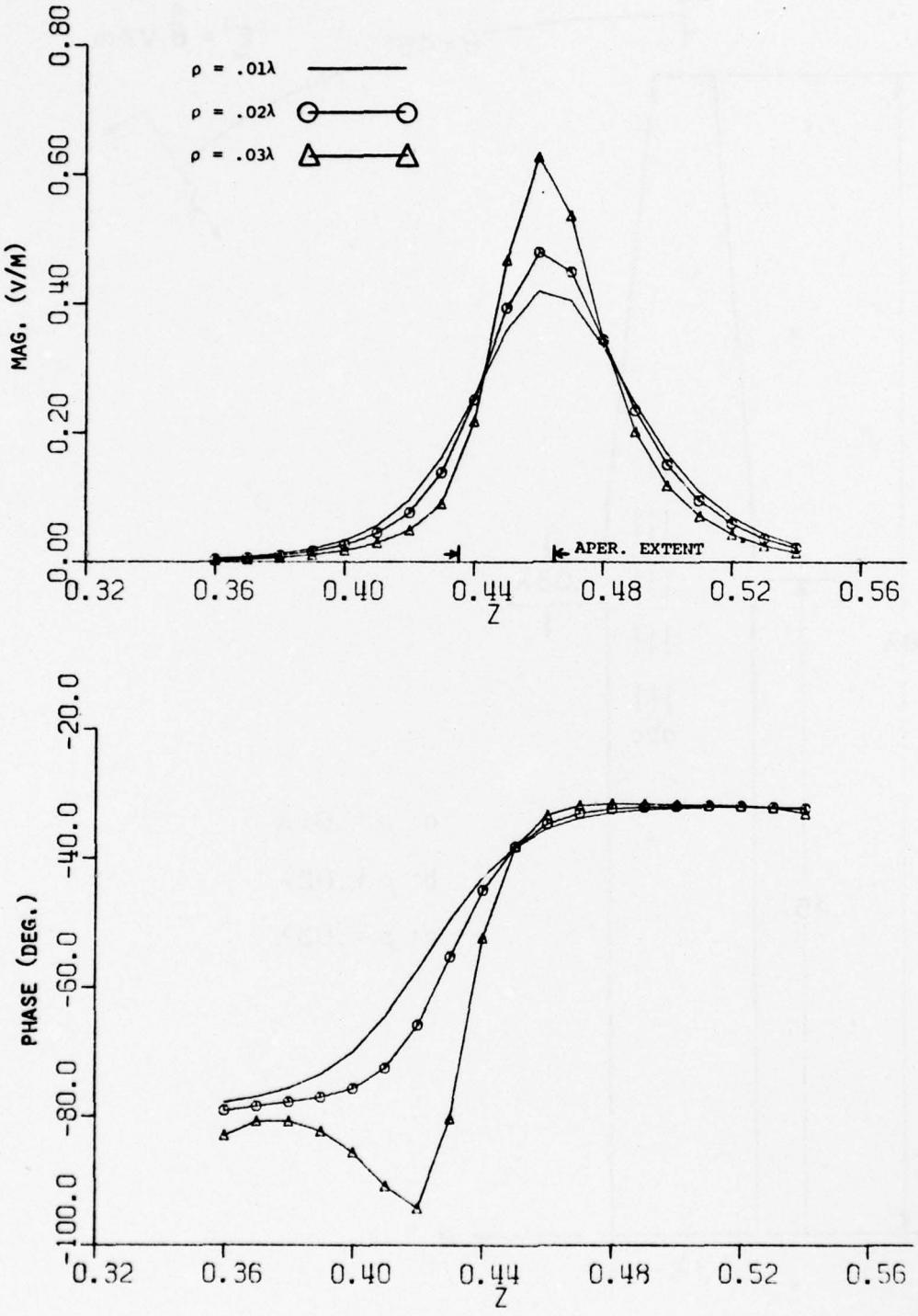

Figure 9. n = 0 Mode$_0$(Uniform in Ø) z Component of Aperture Coupled E-field, E_z.

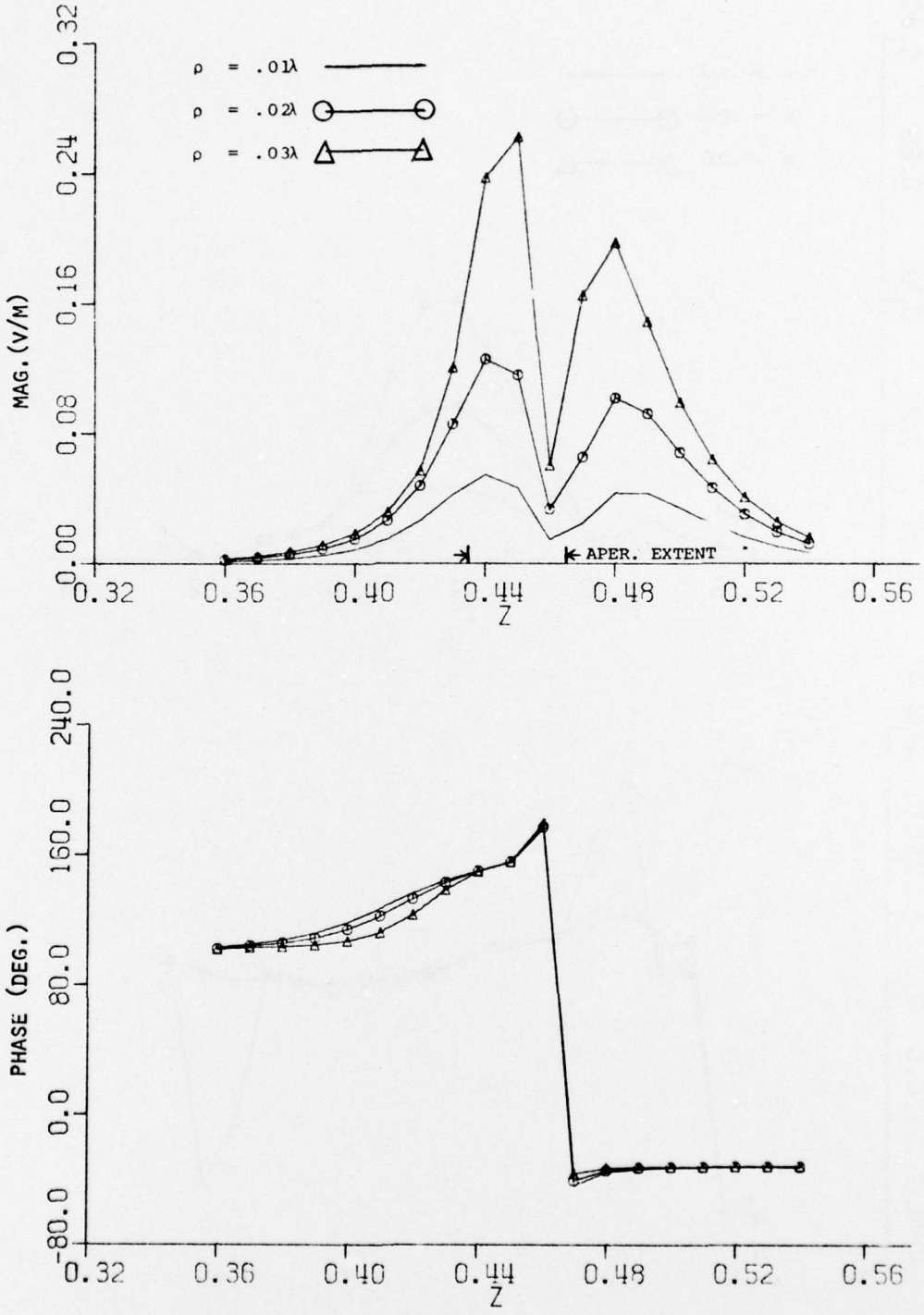

Figure 10. n = 0 Mode (Uniform in Ø) ρ Component of Aperture Coupled E-Field, $\underset{\sim}{E}^0_\rho$.

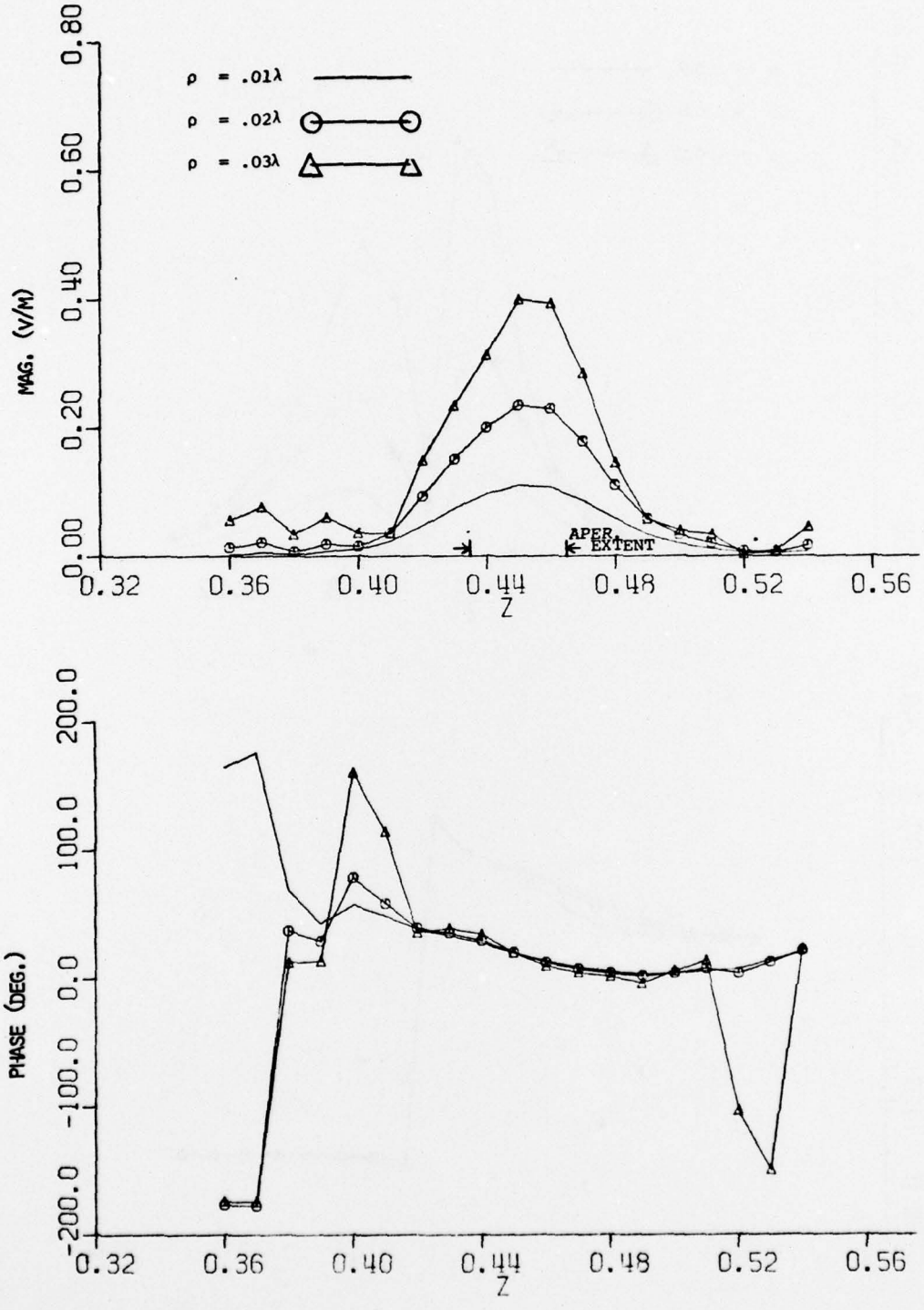

Figure 11. n = 1 Mode (CosØ Varying) z Component of Aperture Coupled E-Field, E^1_z.

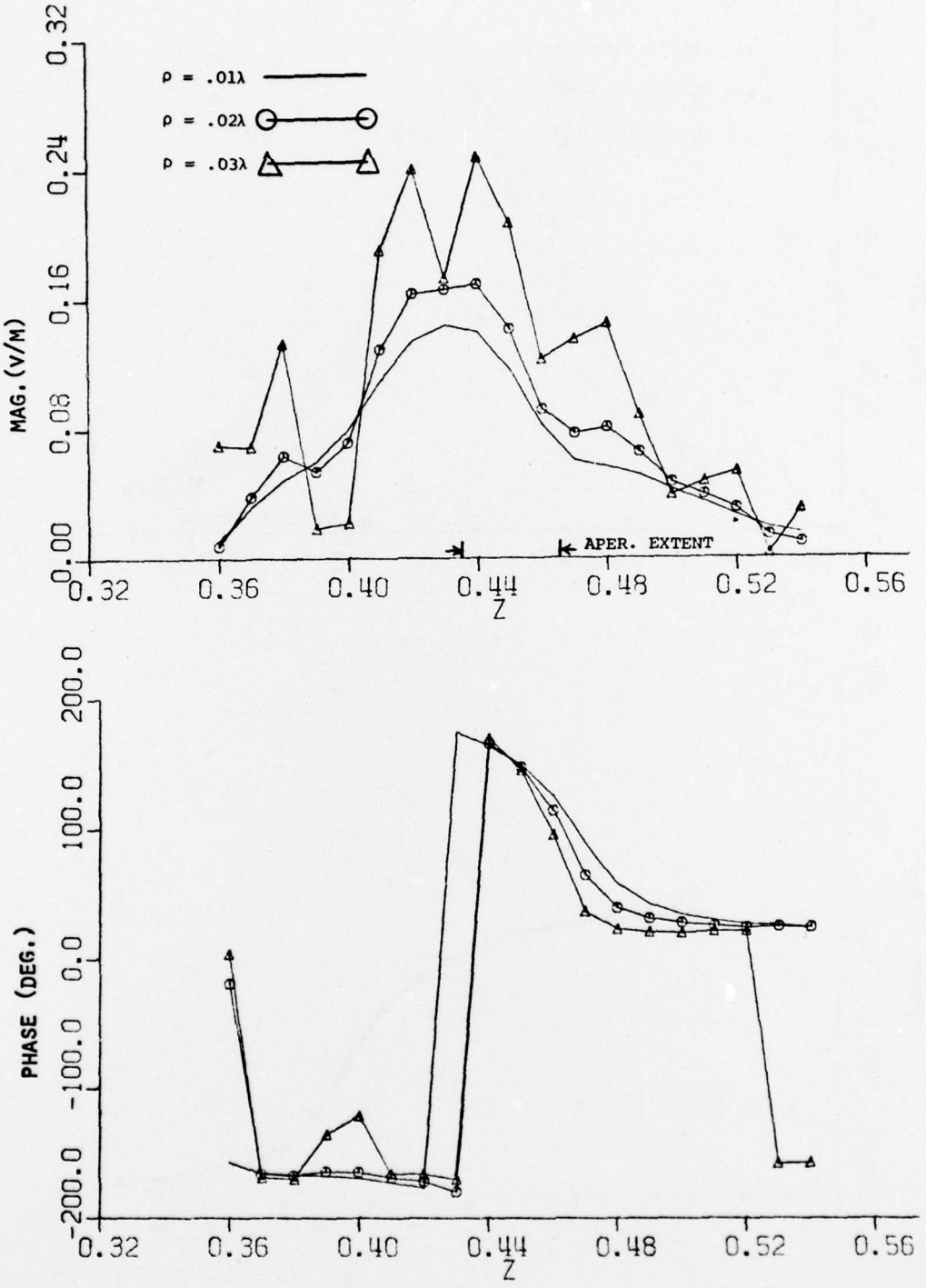

Figure 12. n = 1 Mode (Cosø Varying) ρ Component of Aperture Coupled E-Field, E_ρ^1.

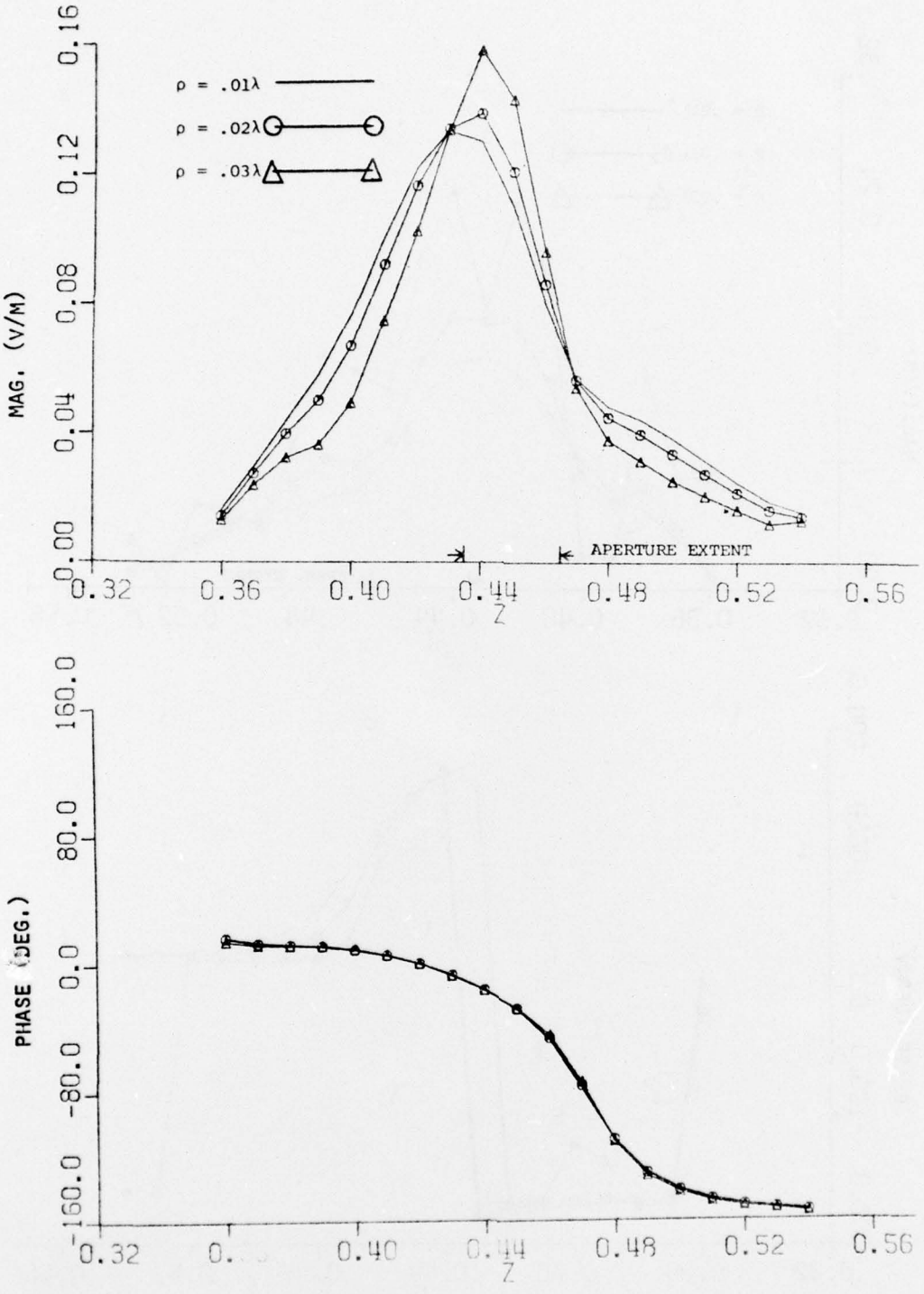

Figure 13. n = 1 Mode (Sinø Varying) ø Component of Aperture Coupled E-Field, E^1_ϕ.

circumferential variation of the n = 1 mode would make it insignificant for far-field scattering it is certainly of significance in aperture coupling.

As expected, E_ρ^0 exhibits a dipole-like behavior (Figure 10). For ρ close to an aperture edge, where the charge density is infinite, E_ρ^0 becomes large. Also the phase of E_ρ^0 changes rapidly in passing by the aperture. The behavior of E_z^0 and E_z^1 are also as expected in that close to the cavity surface they are small (except at the aperture) (Figs. 9, 11) and close to the axis E_z^1 is small. (From symmetry, E_z^1 should vanish along the axis.)

The number of triangle functions used in computing these results was nm = 44. (The corresponding generalized impedance matrix was of order 88 since the current density is bi-directed.) Also, as suggested by the results of Section 4, three triangle peaks were chosen to lie in the thin aperture. This resulted in a 3:1 triangle segment size variation near the aperture.

5.2 Complex Aperture as Equivalent Load

In the beginning of this section it was pointed out that in practice apertures are usually considerably more complex than simple circumferential openings. A typical aperture is depicted in Figure 14. A method for including the effect of the aperture shape and material composition in computing cavity fields is presented here. Essentially it involves the determination of an "aperture load" matrix, $[y_L^A]$, which can be combined with $[y^A]$ such that $\vec{e}$, the column vector representation of $\underset{\sim}{E}^A$, can

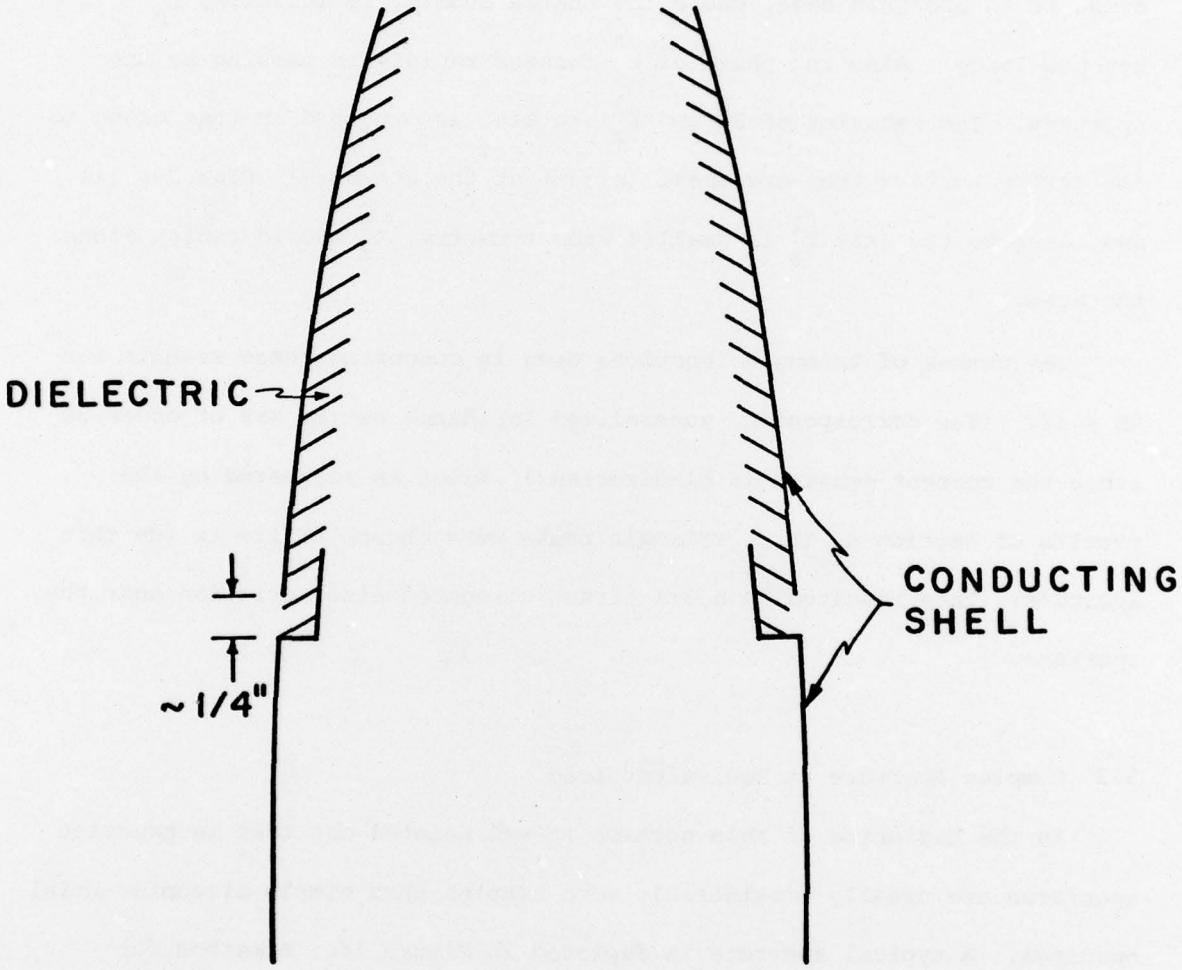

Figure. 14. Typical Circumferential Aperture.

readily be determined.

As discussed in Section 2, both $\vec{j}$, the current vector representation of $\underset{\sim}{J}^A$, and also $[y^A]$ are computed with the aperture "short circuited". Hence, $\vec{j}$ and $[y^A]$ are independent of the aperture complexity (or "loading"). With the aperture present and excited with $\underset{\sim}{J}^A$ (Figure 15a) the problem can be represented in network form as shown in Figure 15b. The generalization of (12) to include the aperture complexity is then

$$\vec{j} = \left([y^A] + [y_L^A]\right) \vec{e} \tag{14}$$

Once $[y_L^A]$ is known, $\vec{e}$ and thus $\underset{\sim}{E}^A$, can be determined from (14). With $\underset{\sim}{E}^A$ known the internal fields can be computed, as before, from a straightforward aperture radiation problem (Figure 15c).

For thin apertures the load matrix elements relating the $\hat{t}$-directed components of current and $\underset{\sim}{E}$-field can be approximated with quasi-static solutions. The shape of the conducting shell at the aperture presents essentially a capacitance the value of which can be approximated by Contour Mapping. Also the conductance and susceptance of material (other than free space) filling the aperture can be determined by mapping methods. The $\hat{\phi}$-directed components of current can easily skirt the thin aperture. Thus only the $\hat{t}$-directed components of loading need be considered.

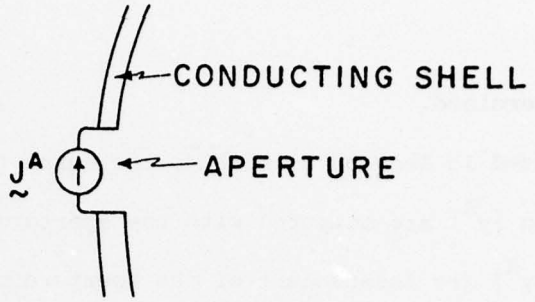

(a)

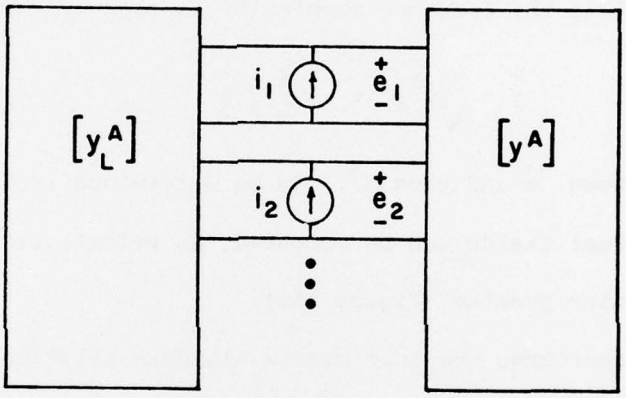

(b)

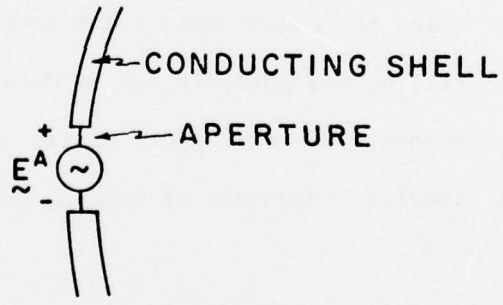

(c)

Figure 15. Aperture Excitation. (a) Current Density Excitation. (b) Network Representation. (c) $\underset{\sim}{E}$-Field Excitation.

6. Conclusions

A moment method for predicting aperture-coupled fields within a rotationally symmetric cavity has been presented. This method, BOR3, employs an equivalent aperture excitation concept which demonstrates greater sensitivity over more conventional procedures if the aperture is thin. This improvement is important, for example, in analyzing the fields coupled through thin circumferential apertures in missile-like structures. A computer program with user manual is available.

APPENDIX A

REVIEW OF METHOD OF MOMENT MODELLING OF A BODY OR REVOLUTION

The necessary relationships for the Harrington-Mautz [1,3] method-of-moment modeling of a body of revolution (BOR) are briefly described here. Only conducting bodies are considered although surface formulations for material bodies exist to which this theory can be extended [7]. This method is based on the $\underset{\sim}{E}$-field formulation. Thus both radiation and scattering problems are solved by a single procedure, and also the thin-walled cavity problem can be handled. The latter is important to aperture coupling considerations.

The $\underset{\sim}{E}$-field formulation relates a free-space surface current density $\underset{\sim}{J}$ to the tangential component of $\underset{\sim}{E}$ along the surface S of a conducting body. In the case of scattering by a perfect conductor

$$\underset{\sim}{E}\Big|_{tan} = \underset{\sim}{E}^{i}\Big|_{tan} + \underset{\sim}{E}^{s}\Big|_{tan} = 0$$

along S where $\underset{\sim}{E}^{i}$ is the impressed field (body absent), $\underset{\sim}{E}^{s}$ is the field radiated by $\underset{\sim}{J}$, and "$|_{tan}$" denotes "component tangential to S". Hence, the $\underset{\sim}{E}$-field formulation becomes

$$\underset{\sim}{E}^{i}\Big|_{tan} = L(\underset{\sim}{J}) \qquad \text{A-1}$$

where

$$L(\underset{\sim}{J}) = -\underset{\sim}{E}^{s}\Big|_{tan} = \left[j\omega\mu \iint_{S} \underset{\sim}{J} \frac{e^{-jkR}}{4\pi R} ds + \frac{\nabla}{j\omega\varepsilon} \iint_{S} (\nabla\cdot\underset{\sim}{J}) \frac{e^{-jkR}}{4\pi R} ds \right]_{tan}$$

Here R is the distance between source and field points on S, the integrations are with respect to the source points, and the remaining symbols have their usual meanings. In the case of radiation $\underset{\sim}{E}|_{tan}$ is known along S and the $\underset{\sim}{E}$-field formulation then becomes

$$-\underset{\sim}{E}|_{tan} = L(\underset{\sim}{J}) \qquad \text{(A-2)}$$

An approximation to $\underset{\sim}{J}$ satisfying (A-1) can be found by the method of moments. Consider the coordinate system of Figure 1. A set of expansion functions $\underset{\sim}{F}^{t}_{nj} = f_j(t)e^{jn\phi}\hat{t}$ and $\underset{\sim}{F}^{\phi}_{nj} = f_j(t)e^{jn\phi}\hat{\phi}$ ($\hat{t}$ and $\hat{\phi}$ are unit vectors) and the symmetric product

$$< J_1, J_2 > = \oint\!\!\!\oint_S \underset{\sim}{J}_1 \cdot \underset{\sim}{J}_2 \, ds = \int_{gc}\int_0^{2\pi} \underset{\sim}{J}_1 \cdot \underset{\sim}{J}_2 \, \rho d\phi dt$$

are chosen. (The "gc" stands for BOR generating curve.) The $f_j(t)$, which express the t variation of the expansion functions, are selected in accordance with the method of subsections [8]. In the Harrington-Mautz BOR model they are triangles (overlapping) divided by the BOR radial coordinate ρ. This choice permits differentiation of the expansion functions and a non-zero value where the poles of the BOR meet the axis. The Fourier components $e^{jn\phi}$ are chosen so that the modal decoupling property of rotationally symmetric bodies applies. Thus for nm triangles on the generating curve $\underset{\sim}{J}$ is expanded as

$$\underset{\sim}{J} = \sum_{n=-\infty}^{\infty} \sum_{j=1}^{nm} (I^{t}_{nj} f_j(t)e^{jn\phi}\hat{t} + I^{\phi}_{nj} f_j(t)e^{jn\phi}\hat{\phi}) \qquad \text{(A-3)}$$

where I_{nj}^{t} and I_{nj}^{ϕ} are the unknown coefficients to be determined such that (A-1) [or (A-2)] is satisfied. The inner product of both sides of (A-1) are taken with respect to each of the weighting functions $\underset{\sim}{W}_{ni}^{t} = f_i(t)e^{-jn\phi}\hat{t}$ and $\underset{\sim}{W}_{ni}^{\phi} = f_i(t)e^{-jn\phi}\hat{\phi}$ resulting in the matrix equation

$$\vec{V}_n = [Z_n]\vec{I}_n \qquad \text{(A-4)}$$

for each n. Upon partitioning, (A-4) becomes

$$\begin{bmatrix} V_n^t \\ \hline V_n^{\phi} \end{bmatrix} = \left[\begin{array}{c|c} [Z_n^{tt}] & [Z_n^{t\phi}] \\ \hline [Z_n^{\phi t}] & [Z_n^{\phi\phi}] \end{array}\right] \begin{bmatrix} \vec{I}_n^t \\ \hline \vec{I}_n^{\phi} \end{bmatrix}$$

With a=t or ϕ the i^{th} element of each $\vec{V}_n^a$ and $\vec{I}_n^a$ subvector is $< W_{ni}^a , E^i >$ and I_{ni}^a respectively. The i,j^{th} element of each $[\Xi_n^{ab}]$ submatrix is $< W_{ni}^a , L F_{nj}^b >$ where ab = tt, ϕt, tϕ, $\phi\phi$.

Each mode of $\underset{\sim}{J}$ is determined independently from (A-3,4) resulting in significant savings in computer processing time and memory. The solution to (A-4) can be expressed as

$$\vec{I}_n = [Y_n]\vec{V}_n \qquad \text{(A-5)}$$

where $[Y_n] = [Z_n]^{-1}$ is the generalized admittance matrix.

The n^{th} mode radiated, or scattered, field $\underset{\sim}{E}_n$ can be determined from (A-5) by reciprocity. A current element $\underset{\sim}{Il}^r$ is located at the field point of interest, $\underset{\sim}{r}$, and oriented parallel to the polarization of interest. If $\vec{V}_n^f$ is the n^{th} mode excitation vector due to $\underset{\sim}{Il}^r$ then

$$\underset{\sim}{E}_n \cdot \underset{\sim}{Il}^r = \tilde{V}_n^f [Y_n] \vec{V}_n \qquad \text{(A-6)}$$

Here $\tilde{V}_n^f$ is the transpose of $\vec{V}_n^f$, $\vec{V}_n^f = \begin{bmatrix} \vec{V}_n^{f^t} \\ \vec{V}_n^{f^\phi} \end{bmatrix}$, the j^{th} element of $\vec{V}_n^{f^a}$ is $< F_{nj}^a, E^r >$ where a = t or ϕ, and $\underset{\sim}{E}^r$ is the field radiated by $\underset{\sim}{I}^r$. Both far [1,3] and near [2] fields can be determined from (A-6).

REFERENCES

[1]. R.F. Harrington and J.R. Mautz, "Radiation and Scattering from Bodies of Revolution," Final Report, prepared for Air Force Cambridge Research Laboratories, Bedford, Mass., under Contract No. F19628-67-C-0233, July 1969.

[2]. R.M. Bevensee, "S3F - SYR/LLL1 The Syracuse Computer Code for Radiation and Scattering from Bodies of Revolution, Extended for Near-Field Computations," Report No. UCRL-51622, prepared for U.S. Atomic Energy Commission under Contract No. W-7405-Eng-48 with the Lawrence Livermore Laboratory, University of California, Livermore, CA, May 1974.

[3]. J.R. Mautz and R.F. Harrington, "Generalized Network Parameters for Bodies of Revolution," Scientific Report No. 1, Contract No. F-19628-67-C-0233, Air Force Cambridge Research Laboratories, Bedford, Mass., with Syracuse University, Syracuse, N.Y., May 1968. Or see instead: J.R. Mautz and R.F. Harrington, "Radiation and Scattering from Bodies of Revolution," Applied Scientific Research, Vol. 20, 1969.

[4]. S.A. Schelkunoff, "Field Equivalence Theorems," Comm. on Pure and Applied Math., Vol. 4, pp. 43-59, June 1951.

[5]. H.K. Schuman, "Coupling Through Non-Azimuthally Symmetric Apertures in a Body-of-Revolution", Internal Memorandum, Dept. of Electrical and Computer Engineering, Syracuse University, July 1974.

[6]. T.B.A. Senior and G.A. Desjardins, "Electromagnetic Field Penetration into a Spherical Cavity," IEEE Trans. on Electromagnetic Compatibility, Vol. EMC-16, pp. 205-208, November 1974.

[7]. Private Communications with 1) L.L. Tsai and T.K. Wu at the University of Mississippi, Oxford, Mississippi, and 2) R.F. Harrington and J.R. Mautz at Syracuse University, Syracuse, New York.

[8]. R.F. Harrington, Field Computation by Moment Methods, The Macmillan Co., New York, 1968.

[9]. H.K. Schuman, "Coupling through Rotationally Symmetric Apertures in Cavities of Revolution - Computer Code (BOR3) Description", Tech Memo, Electrical and Computer Engineering Dept., Syracuse University, Syracuse, NY 13210, September, 1976.